Unequal Power Division Ratio Nonreciprocal Filtering Power Divider With Arbitrary Termination Impedance and Center Frequency Tunability

Girdhari Chaudhary, *Member, IEEE*, and Yongchae Jeong, *Senior Member, IEEE*

***Abstract*— This article presents RF design and practical implementation of a nonreciprocal filtering power divider that enables arbitrary power division ratio (k^2) and center frequency tunability. By modulating resonators in the filtering power divider with progressive phase shift sinusoidal modulation signals, a nonreciprocal response ($|S_{21}| \neq |S_{12}|$ and $|S_{31}| \neq |S_{13}|$) is achieved. The analytical spectral S-parameters of nonreciprocal filtering power divider have been derived for insight analytical nonreciprocal frequency response and practical implementation. The proposed analytical equations can be applied to design a nonreciprocal filtering power divider with arbitrary k^2 and any arbitrary termination port impedances. Center frequency tunability can be achieved by tuning the resonant frequencies of time-modulated resonators. For experimental validation, prototypes of nonreciprocal filtering power dividers with $k^2 = 1$ and $k^2 = 0.5$ are designed, implemented, and manufactured. The measured results confirm the accuracy of the analytical design equations. In the experimental results, the center frequency of nonreciprocal filtering power dividers is tuned from 1.66 to 1.98 GHz (17.58%) with a maximum forward insertion loss of 4.95 dB and reverse isolation ($|S_{12}|$ and $|S_{13}|$) higher than 20 dB at each center frequency tuning state.**

***Index Terms*— Arbitrary power division ratio, frequency tunable, intermodulation (IM) products, isolator, nonreciprocal filtering power divider, time-modulated resonators, unequal power division ratio.**

I. Introduction

POWER dividers/combiners and filters are key components of modern wireless communication systems, such as phased array antenna systems and in-band full-duplex (IBFD) systems [1], [2]. However, these conventional power dividers/combiners are reciprocal in nature governed by the Lorentz reciprocity theorem [3]. Today's state-of-the-art and next-generation wireless communication systems demand cost-effective, miniaturized, integrated solutions of multifunctional components in a single device. Designing multifunctional components, such as nonreciprocal filtering power dividers with tunable center frequency, has attracted significant interest as this component opens the door for a wide range application in the next-generation radar, imaging, and communication systems. Merging the nonreciprocal response of the power divider with the antenna will allow independent control of transmission and reception properties of phased array antenna at the same operation frequency, which pave the way to new functionalities and applications in radar, sensing, and IBFD communication systems [4], [5].

Traditionally, nonreciprocal components such as circulator and isolator have been mainly designed by breaking the nonreciprocity with ferrite magnetic materials, which are bulky, expensive, and incompatible with integrated circuits [6], [7], [8]. To eliminate the use of a magnet, active and nonlinear circuit approaches have been applied to design nonreciprocal components; however, these approaches suffer from poor noise figure, limited power handling, and small dynamic range [9], [10], [11].

In recent years, magnetless nonreciprocal circuits have been widely investigated based on different approaches such as linear periodically time-varying (LPTV) circuits approach, staggered commutation, spatiotemporal modulation (STM) approach, in pursuit of integration, affordability, and miniaturization [12], [13], [14], [15], [16]. Magnetless nonreciprocal bandpass filters (BPFs) that allow a signal travel in only direction have been designed using time-modulated resonators. In [17], [18], and [19], nonreciprocal BPFs have been presented using a lumped element time-modulated resonator. Modulating capacitor within the resonator generates intermodulation (IM) products and the significant difference between the RF power distribution among IM products in forward and reverse direction paths generated nonreciprocity [17], [20]. A time-varying coupling matrix approach was generalized in [21] to design nonreciprocal BPF. However, these works employed a low-pass filter (LPF) and static dc block capacitor to separate the modulation signal and RF signal, which can increase complexity in the practical implementation of additional dc

Manuscript received 29 March 2023; revised 16 May 2023; accepted 5 June 2023. Date of publication 3 July 2023; date of current version 10 January 2024. This work was supported in part by the National Research Foundation of Korea (NRF) Grant funded by Korea Government [Ministry of Science and ICT (MSIT)] under Grant RS-2023-00209081; in part by Basic Science Research Program through the NRF of Korea, funded by Ministry of Education, under Grant 2019R1A6A1A09031717; and in part by Research Base Construction Fund Support Program funded by Jeonbuk National University in 2022. *(Corresponding author: Yongchae Jeong.)*

The authors are with the JIANT-IT Human Resource Development Center, Division of Electronic and Information Engineering, Jeonbuk National University, Jeonju, Jollabuk-do 54896, Republic of Korea (e-mail: girdharic@jbnu.ac.kr; ycjeong@jbnu.ac.kr).

Color versions of one or more figures in this article are available at https://doi.org/10.1109/TMTT.2023.3288635.

Digital Object Identifier 10.1109/TMTT.2023.3288635

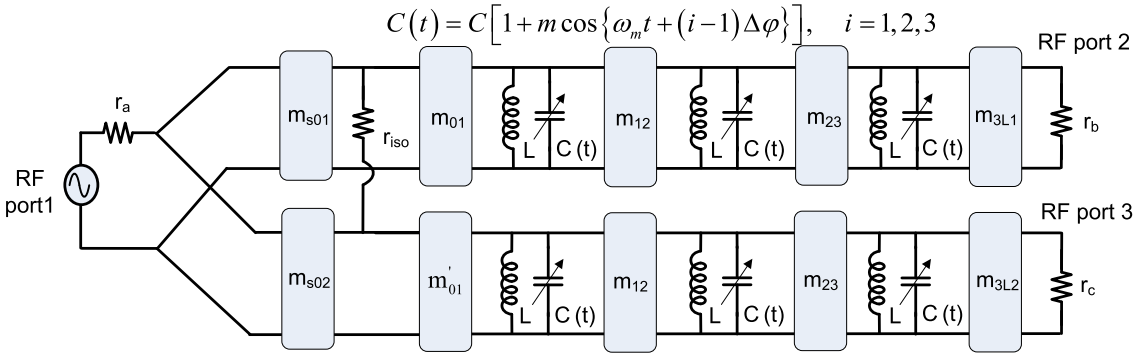

Fig. 1. Proposed structure of arbitrary terminated nonreciprocal power divider with 1: k^2 power division ratio and tunable center frequency.

bias and duplexing circuits. In [22], [23], [24], and [25], nonreciprocal BPFs have been implemented in microstrip line using half-wavelength and quarter wavelength time-modulated resonators.

In [26], a nonreciprocal power divider based on photonic topological insulators is investigated, but only numerical simulation results have been provided. Most recently, a nonreciprocal filtering power divider based on time-modulated resonators is presented in [27]. However, this design method is only applicable for equal power division ratio and provides narrowband reverse isolation.

In this work, we propose a nonreciprocal filtering power divider based on time-modulated resonators that offer arbitrary power division ratio, frequency tunability, and the ability to behave as an impedance transformer, filtering power divider, and isolator function in a single circuit. Analytical spectral S-parameters have been derived to gain insight into nonreciprocity in filtering power divider. The proposed design equations are applicable for arbitrary k^2 as well as arbitrary termination port impedances. To achieve nonreciprocity in the microstrip line filtering power divider, the progressive phase-shift sinusoidal modulation signal is directly applied to the varactor diode through a bias transmission line (TL), simplifying the practical implementation of the modulation circuit. The frequency tunable nonreciprocal response is achieved by tuning the bias voltage of the varactor diode and modulation parameters.

II. Design Theory

Fig. 1 shows the proposed structure of an arbitrary k^2 nonreciprocal power divider with a tunable center frequency. The proposed nonreciprocal power divider is terminated with arbitrary impedances r_a, r_b, and r_c, where the termination impedances are normalized to 50 Ω. To achieve a nonreciprocal response, we apply a sinusoidal modulation signal with a progressive phase shift to modulate the capacitors of the filtering power divider, as shown in Fig. 1, which makes the system nonlinear [17], [21]. The capacitors of the nonreciprocal power divider are modulated with progressive phase-shift sinusoidal modulation signal as follows [15]:

$$C(t) = C\left[1 + \xi\cos\{2\pi f_m t + (i-1)\Delta\varphi\}\right], \quad i = 1, 2, 3 \tag{1}$$

where f_{m} is the modulation frequency of the signal, $\Delta\varphi$ is the progressive phase shift, and ξ is the modulation index. Likewise, C is the nominal capacitance. The phase difference ($\Delta\varphi$) is the key mechanism that enables a nonreciprocal response. Each resonator generates a number of nonlinear harmonics, which are coupled by time-modulated capacitors. For simplicity, considering only two nonlinear harmonics [17], the spectral admittance matrix of each resonator is given as in (2), shown at the bottom of the page, where

$$x^n = 2\pi(f + nf_m), \quad n = -2, -1, 0, +1, +2. \tag{3}$$

A. Even-Mode Equivalent Circuit Analysis

Fig. 2 depicts the equivalent circuit of the nonreciprocal power divider under even-mode excitation. Assuming a power division ratio of 1: k^2, the termination impedance r_a at port 1 is divided into $r_{\mathrm{e}12}$ and $r_{\mathrm{e}13}$, as shown in Fig. 2, and expressed as follows:

$$r_{\mathrm{e}12} = r_a\left(\frac{1+k^2}{k^2}\right), \quad r_{\mathrm{e}13} = r_a\left(1+k^2\right). \tag{4}$$

The values of the coupling element value ($m_{\mathrm{s}01}$, $m_{\mathrm{s}02}$, m_{01}, and so on) possess the same value under progressive

$$\lambda_i = j\begin{bmatrix} x^{-2}C - \frac{1}{x^{+2}L} & x^{-2}C\frac{\xi}{2}e^{-j(i-1)\Delta\varphi} & 0 & 0 & 0 \\ x^{-1}C\frac{\xi}{2}e^{j(i-1)\Delta\varphi} & x^{-1}C - \frac{1}{x^{-1}L} & x^{-1}C\frac{\xi}{2}e^{-j(i-1)\Delta\varphi} & 0 & 0 \\ 0 & x^{0}C\frac{\xi}{2}e^{j(i-1)\Delta\varphi} & x^{0}C - \frac{1}{x^{0}L} & x^{0}C\frac{\xi}{2}e^{-j(i-1)\Delta\varphi} & 0 \\ 0 & 0 & x^{+1}C\frac{\xi}{2}e^{j(i-1)\Delta\varphi} & x^{+1}C - \frac{1}{x^{-1}L} & x^{+1}C\frac{\xi}{2}e^{-j(i-1)\Delta\varphi} \\ 0 & 0 & 0 & x^{+2}C\frac{\xi}{2}e^{j(i-1)\Delta\varphi} & x^{+2}C - \frac{1}{x^{+2}L} \end{bmatrix}, \quad i = 1, 2, 3 \tag{2}$$

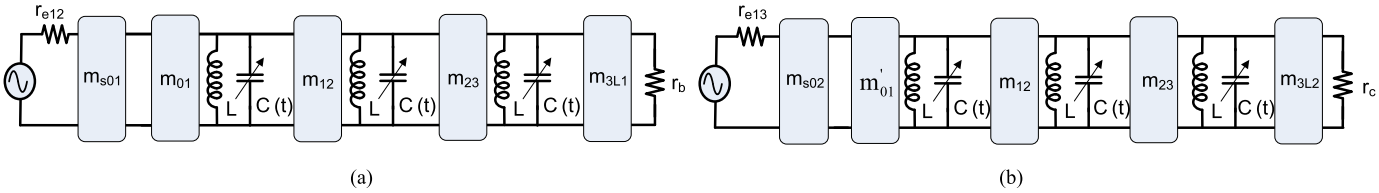

Fig. 2. Equivalent circuit of the proposed nonreciprocal power divider under even-mode excitation: (a) between ports 1 and 2 and (b) between ports 1 and 3.

phase-shift sinusoidal modulation of resonators [21]. As a result, the normalized values of the coupling elements are given as follows:

$$m_{s01}=\sqrt{\frac{k^2}{r_a r_b\left(1+k^2\right)}},\quad m_{s02}=\sqrt{\frac{1}{r_a r_b\left(1+k^2\right)k^2}} \tag{5a}$$

$$m_{01}=\frac{1}{\sqrt{r_b g_0 g_1}},\quad m'_{01}=\frac{1}{\sqrt{k^2 r_b g_0 g_1}},\quad m_{12}=\frac{1}{\sqrt{g_1 g_2}} \tag{5b}$$

$$m_{23}=\frac{1}{\sqrt{g_2 g_3}},\quad m_{3L1}=\frac{1}{\sqrt{g_3 g_4 r_b}},\quad m_{3L2}=\frac{1}{\sqrt{g_3 g_4 r_c}} \tag{5c}$$

where g_i is the LPF prototype element values [28]. Assuming bandwidth (Δ) and center frequency (f_0) of the proposed nonreciprocal power divider, the values of C and L of the resonator are given as (6) if termination impedances are normalized to 50 Ω:

$$C=\frac{1}{2\pi\Delta},\quad L=\frac{1}{4\pi f_0^2 C}. \tag{6}$$

Once the spectral admittance of time-modulated resonators and coupling element values are determined using (2)–(5), the spectral S-parameters of the nonreciprocal filtering power divider can be obtained using the following equation (7) and as in (8), shown at the bottom of the page.

$$\mathbf{S_{11}}=\frac{\mathbf{b}_3-r_s\left(1+k^2\right)\mathbf{m_{s01}^2}\left(r_b\mathbf{m_{3L1}^2}\mathbf{b}_1+\mathbf{b}_2\right)}{\mathbf{b}_3+r_s\left(1+k^2\right)\mathbf{m_{s01}^2}\left(r_b\mathbf{m_{3L1}^2}\mathbf{b}_1+\mathbf{b}_2\right)} \tag{7a}$$

$$\mathbf{S_{22}}=U-2\left[U+\frac{U}{\mathbf{b}_5}\left\{k^2\mathbf{m_{01}^2}\mathbf{b}_4+r_s\left(1+k^2\right)\mathbf{m_{s01}^2}\mathbf{b}_2\right\}\right]^{-1} \tag{7b}$$

$$\mathbf{S_{33}}=U-2\left[U+\frac{U}{\mathbf{b}_6}\left\{\mathbf{m_{01}'^2}\mathbf{b}_4+r_s\left(1+k^2\right)\mathbf{m_{s02}^2}\mathbf{b}_2\right\}\right]^{-1} \tag{7c}$$

where

$$\mathbf{b}_1=\mathbf{m_{12}^2}U+\lambda_1\lambda_2,\ \mathbf{b}_2=\mathbf{m_{23}^2}\lambda_1+\mathbf{m_{12}^2}\lambda_3+\lambda_1\lambda_2\lambda_3 \tag{9a}$$

$$\mathbf{b}_3=k^2\mathbf{m_{01}^2}\left(r_b\mathbf{m_{3L1}^2}\lambda_2+\mathbf{m_{23}^2}+\lambda_2\lambda_3\right) \tag{9b}$$

$$\mathbf{b}_4=\mathbf{m_{23}^2}+\lambda_2\lambda_3 \tag{9c}$$

$$\mathbf{b}_5=k^2 r_b\mathbf{m_{3L1}^2}\mathbf{m_{01}^2}\lambda_2+r_b r_s\left(1+k^2\right)\mathbf{m_{3L1}^2}\mathbf{m_{s01}^2}\mathbf{b}_1 \tag{9d}$$

$$\mathbf{b}_6=r_c\mathbf{m_{3L2}^2}\mathbf{m_{01}'^2}\lambda_2+r_c r_s\left(1+k^2\right)\mathbf{m_{3L2}^2}\mathbf{m_{s02}^2}\mathbf{b}_1 \tag{9e}$$

$$\mathbf{b}_7=k^2 r_b\mathbf{m_{01}^2}\mathbf{m_{3L1}^2}\lambda_2+k^2\mathbf{m_{01}^2}\mathbf{b}_4 \tag{9f}$$

$$\mathbf{b}_8=r_s\left(1+k^2\right)\mathbf{m_{s01}^2}\left(r_b\mathbf{m_{3L1}^2}\mathbf{b}_1+\mathbf{b}_2\right) \tag{9g}$$

$$\mathbf{b}_9=\mathbf{m_{01}}\mathbf{m_{3L1}}\left(r_b\mathbf{m_{3L1}^2}\lambda_2+\mathbf{b}_4\right) \tag{9h}$$

$$\mathbf{b}_{10}=r_c\mathbf{m_{01}'^2}\mathbf{m_{3L2}^2}\lambda_2+\mathbf{m_{01}'^2}\mathbf{b}_4 \tag{9i}$$

$$\mathbf{b}_{11}=r_s\left(1+k^2\right)\mathbf{m_{s02}^2}\left(r_c\mathbf{m_{3L2}^2}\mathbf{b}_1+\mathbf{b}_2\right) \tag{9j}$$

$$\mathbf{b}_{12}=\mathbf{m'_{01}}\mathbf{m_{3L2}}\left(r_c\mathbf{m_{3L2}^2}\lambda_2+\mathbf{b}_4\right). \tag{9k}$$

The values of the coupling element are $\mathbf{m_{s01}}=m_{s01}U$, $\mathbf{m_{s02}}=m_{s02}U$, $\mathbf{m_{01}}=m_{01}U$, $\mathbf{m'_{01}}=m'_{01}U$, $\mathbf{m_{12}}=m_{12}U$, $\mathbf{m_{23}}=m_{23}U$, $\mathbf{m_{3L1}}=m_{3L1}U$, and $\mathbf{m_{3L2}}=m_{3L2}U$, and U is the unity matrix. The value of the spectral admittance matrix λ_i is given in (2).

The nonreciprocal response of the filtering power divider ($|\mathbf{S_{21}}|\neq|\mathbf{S_{12}}|$ and $|\mathbf{S_{31}}|\neq|\mathbf{S_{13}}|$) arises from the difference between (7a) and (7b) and (7c) and (8d), which is due to the generation of IM products caused by STM. It should be noted that only central elements in matrices presented in (8) and (7) represent the fractional power conversion at the fundament frequency; other elements represent the interharmonic spectral power conversion. In fact, all elements collectively contribute to achieving nonreciprocal response at the fundamental frequency. When λ_i values of all the resonators are the same, the proposed filtering power divider provides a reciprocal response resulting in $|S_{21}|=|S_{12}|$ and $|S_{31}|=|S_{13}|$.

$$\mathbf{S_{21}}=\frac{2\sqrt{k^2 r_a r_b}\mathbf{m_{s01}}\mathbf{m_{01}}\mathbf{m_{12}}\mathbf{m_{23}}\mathbf{m_{3L1}}}{k^2 r_b\mathbf{m_{01}^2}\mathbf{m_{3L1}^2}\lambda_2+k^2\mathbf{m_{01}^2}\mathbf{b}_4+r_a\left(1+k^2\right)\mathbf{m_{s01}^2}\left(r_b\mathbf{m_{3L1}^2}\mathbf{b}_1+\mathbf{b}_2\right)} \tag{8a}$$

$$\mathbf{S_{12}}=\frac{2}{1+k^2}\sqrt{\frac{k^2 r_b}{r_a}}\left[\frac{\mathbf{b}_8}{\mathbf{b}_8+\mathbf{b}_7}\right]\times\left[\frac{\mathbf{m_{01}}\mathbf{m_{3L1}}\lambda_2}{\mathbf{m_{s01}}\mathbf{m_{12}}\mathbf{m_{23}}}-\left\{\frac{\mathbf{b}_9}{\mathbf{m_{s01}}\left(r_b\mathbf{m_{3L1}^2}\mathbf{b}_1+\mathbf{b}_2\right)}\right\}\left\{\frac{\mathbf{b}_1}{\mathbf{m_{12}}\mathbf{m_{23}}}\right\}\right] \tag{8b}$$

$$\mathbf{S_{31}}=\frac{2\sqrt{k^2 r_a r_c}\mathbf{m_{s02}}\mathbf{m'_{01}}\mathbf{m_{12}}\mathbf{m_{23}}\mathbf{m_{3L2}}}{r_c\mathbf{m_{01}'^2}\mathbf{m_{3L2}^2}\lambda_2+\mathbf{m_{01}'^2}\mathbf{b}_4+r_a\left(1+k^2\right)\mathbf{m_{s02}^2}\left(r_c\mathbf{m_{3L2}^2}\mathbf{b}_1+\mathbf{b}_2\right)} \tag{8c}$$

$$\mathbf{S_{13}}=\frac{2}{1+k^2}\sqrt{\frac{k^2 r_c}{r_a}}\left[\frac{\mathbf{b}_{11}}{\mathbf{b}_{11}+\mathbf{b}_{10}}\right]\left\{\frac{\mathbf{m'_{01}}\mathbf{m_{3L2}}\lambda_2}{\mathbf{m_{s02}}\mathbf{m_{12}}\mathbf{m_{23}}}-\left\{\frac{\mathbf{b}_{12}}{\mathbf{m_{s02}}\left(r_c\mathbf{m_{3L2}^2}\mathbf{b}_1+\mathbf{b}_2\right)}\right\}\left\{\frac{\mathbf{b}_1}{\mathbf{m_{12}}\mathbf{m_{23}}}\right\}\right\}. \tag{8d}$$

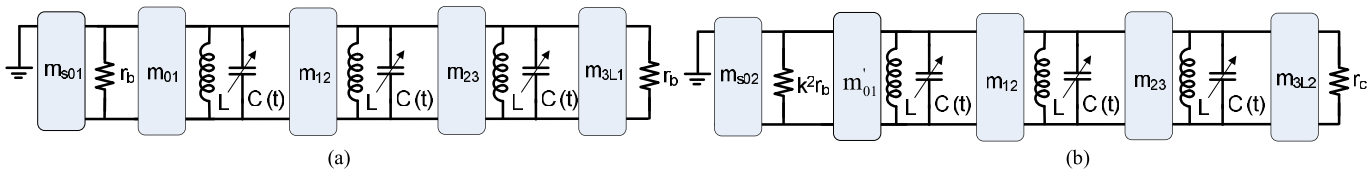

Fig. 3. Equivalent circuit of the proposed nonreciprocal power divider under odd-mode excitation: (a) between ports 1 and 2 and (b) between ports 1 and 3.

B. Odd-Mode Equivalent Circuit Analysis

Fig. 3 depicts the equivalent circuit of the proposed filtering power divider under odd-mode excitation. As the termination impedance of port 1 is short-circuited under odd-mode excitation, there is no signal transmission to output ports 2 and 3. Under odd-mode excitation, the normalized isolation resistors between output ports are given as follows:

$$r_{\text{iso}}^{21} = r_b, \quad r_{\text{iso}}^{31} = k^2 r_b. \tag{10}$$

To achieve infinite isolation ($|S_{23}| = 0$) between ports 2 and 3, the values of r_{iso}^{21} and r_{iso}^{31} should be transformed to r_b and r_c, which are termination impedance at ports 2 and 3, respectively, as shown in the equivalent circuit of nonreciprocal filtering power divider in Fig. 3. Therefore, the normalized isolation resistor (r_{iso}) that can achieve infinite isolation between output ports of nonreciprocal filtering power divider can be found using the following equation:

$$r_{\text{iso}} = r_b\left(1 + k^2\right). \tag{11}$$

From (11), it can be noted that the value of the normalized isolation resistor depends on the termination impedance (r_b) of port 2 and the power division ratio (k^2) of the nonreciprocal filtering power divider and provide infinite isolation between output ports.

C. Modulation Parameters Extraction

To demonstrate the design equations, the results of numerical simulations are shown in Figs. 4 and 5. Fig. 4 illustrates the simulated forward transmission ($|S_{21}|$, $|S_{31}|$), reverse isolation ($|S_{12}|$, $|S_{13}|$), and input/output return losses (RLs) ($|S_{ii}|$, i= 1, 2, 3) as a function of modulation frequency. Similarly, Fig. 5 presents the calculated S-parameters at f_0 and 20-dB isolation bandwidth for various modulation parameters (f_{m}, ξ, and $\Delta\varphi$). The design specifications for the nonreciprocal filtering power divider are given as $f_0 = 1.80$ GHz and equiripple bandwidth (Δ) of 100 MHz. The prototype element values for the Chebyshev filter response [28] are given as $g_0 = g_4 = 0.84985$, $g_1 = g_3 = 0.8635$, and $g_2 = 1.1038$.

In Fig. 4, it is observed that the f_{m} should be chosen nearly equal to the equiripple bandwidth of the filtering power divider which creates two nulls in $|S_{12}|$ and $|S_{13}|$ curves. When f_{m} < equiripple bandwidth, the separation between the two nulls in $|S_{12}|$ and $|S_{13}|$ curves converges to a single null with high reverse isolation only at f_0. On the other hand, when f_{m} > equiripple bandwidth, the separation between the two nulls in $|S_{12}|$ and $|S_{13}|$ increases, but the magnitude at f_0 is degraded.

As shown in Fig. 5, the forward transmission ($|S_{21}|$ and $|S_{31}|$) insertion loss (IL) is slightly affected by the modulation frequency (f_{m}). However, reverse isolation (IX = $|S_{12}|$ and $|S_{13}|$) has only one null at f_0 and the 20-dB IX bandwidth is narrow when f_{m} is smaller than the equiripple bandwidth of the filtering power divider. On the other hand, the 20-dB IX bandwidth increases when f_{m} is higher than the equiripple bandwidth, but IX = $|S_{12}|$ and $|S_{13}|$ at f_0 is degraded. The tradeoff exists between 20-dB IX bandwidth and IX at f_0. The reverse IX increases as the modulation index (ξ) increases, but forward transmission IL, 20-dB IX bandwidth, and RL are degraded. Similarly, the reverse IX slightly increases as the progressive phase shift ($\Delta\varphi$) increases, but 20-dB IX bandwidth and RL are degraded. Based on the above discussion, f_{m} should select nearly equal to the equiripple bandwidth of the nonreciprocal filtering power divider for optimum electrical performance. The $\Delta\varphi$ should be chosen between 50° and 70°.

D. Design Examples: Frequency Response of Nonreciprocal Filtering Power Divider

Numerical simulations are carried out using the design equations discussed in the previous section, and the results are presented in Fig. 6. The filter specification is the same as previously described in Section II-C, and the modulation parameters are chosen as $f_{\text{m}} = 102$ MHz, $\zeta = 0.10$, and $\Delta\varphi = 60°$. The nonreciprocal response ($|S_{21}| \neq |S_{12}|$ and $|S_{31}| \neq |S_{13}|$) achieved in all cases ($k^2 = 0.5$, 0.75, and 1). These results showed that the forward IL (excluding the intrinsic loss of the power divider) < 0.7 dB, input/output RLs > 16 dB, and reverse IX ($|S_{12}|$, $|S_{13}|$) > 20 dB within passband frequency, and isolation between output ports ($|S_{23}|$) is infinite. The forward transmission IL is due to power conversion to IM products. Furthermore, two transmission zeros (TZs) are generated in the forward transmission. These TZs are generated because the transversal of RF energy occurs not only through the adjacent resonators at fundamental frequency but also through nonadjacent resonators at harmonic frequencies. The proper selection of modulation parameters resulted in an excellent nonreciprocal response. Fig. 7 shows the numerical simulation results of a nonreciprocal power divider with different equiripple bandwidths (Δ). As noted from these results, modulation frequency (f_{m}) and modulation index (ξ) increase as the Δ increases.

It is worth noting that the frequency tunability of the nonreciprocal filter power divider is achieved by tuning resonant frequencies of time-modulated resonators. Fig. 8 presents the numerical simulation results demonstrating the frequency tunability characteristics. The center frequency is tuned from 1.60 to 2 GHz in all cases ($k^2 = 0.25$, 1, and 2) with forward IL (excluding intrinsic loss of power divider) < 0.7 dB, reverse IX > 20 dB within passband frequency, and RL > 16 dB.

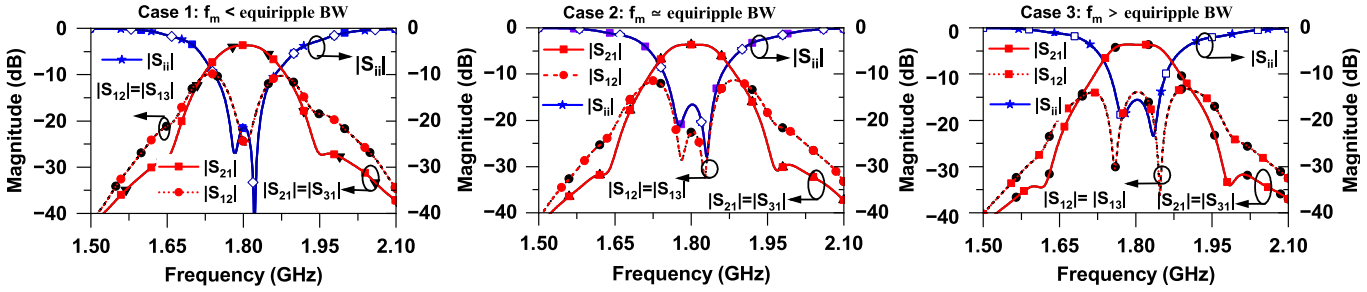

Fig. 4. Simulated frequency response of nonreciprocal filtering power divider with a different modulation frequency (f_{m}). Other specifications: $f_0 = 1.8$ GHz and $\Delta = 100$ MHz, and LPF prototype element values: $g_0 = g_4 = 0.84985$, $g_1 = g_3 = 0.8635$, and $g_2 = 1.1038$. Modulation parameters: $\xi = 0.10$ and $\Delta\varphi = 60°$ and different f_{m}.

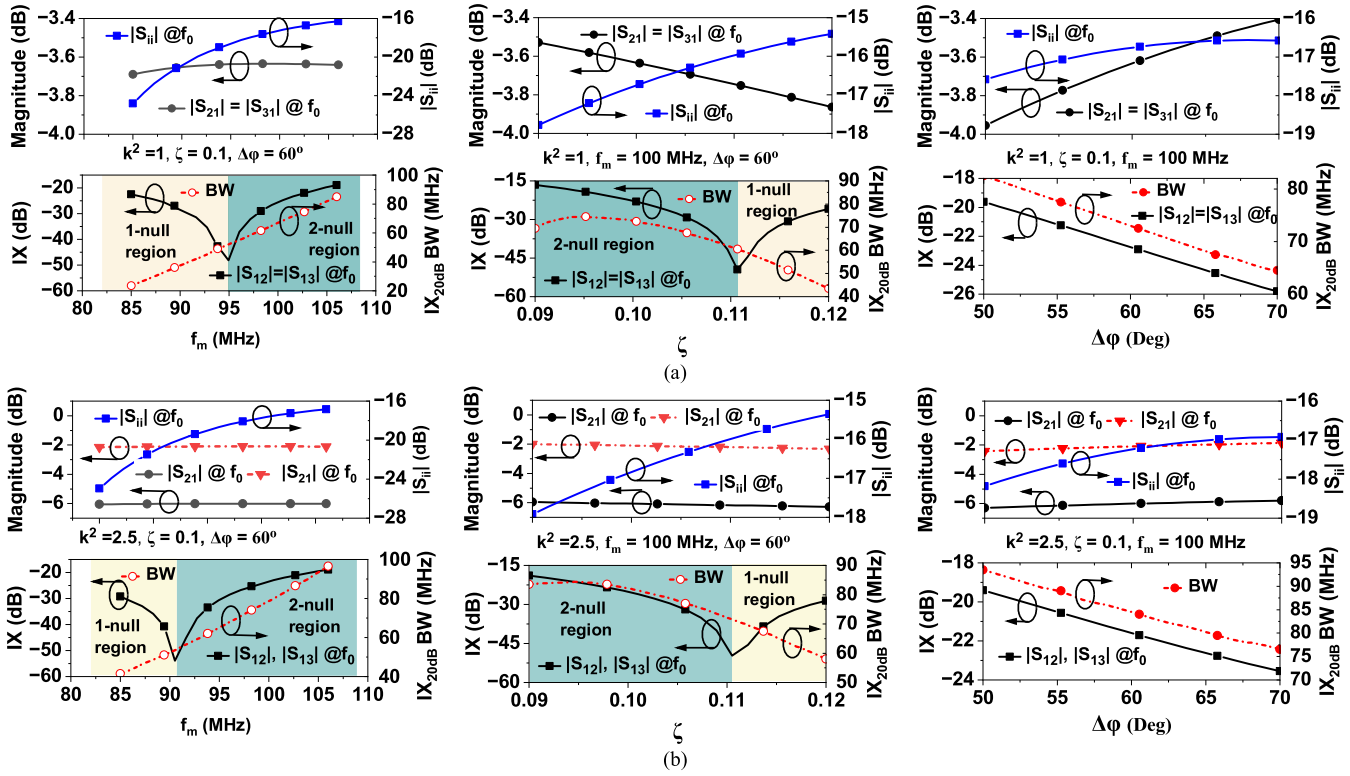

Fig. 5. Calculated forward transmission and reverse isolation at center frequency according to modulation parameters: f_{m}, ξ, and $\Delta\varphi$: (a) equal power division ratio ($k^2 = 1$) and (b) unequal power division ratio ($k^2 = 2.5$). LPF prototype elements: $g_0 = g_4 = 0.84985$, $g_1 = g_3 = 0.8635$, $g_2 = 1.1038$, and $f_0 = 1.80$ GHz and equiripple bandwidth of nonreciprocal filtering power divider (Δ) = 100 MHz. Reverse isolation (IX) represents the magnitude of $|S_{12}|$ and $|S_{13}|$.

The isolation between output ports is not shown in Fig. 8 because of its infinite theoretical value.

III. Experimental Results

For the experimental demonstration, a prototype of microstrip line nonreciprocal filtering power dividers with $k^2 = 1$ and $k^2 = 0.5$ is designed and fabricated on a Taconic substrate with a dielectric constant of 2.2, thickness of 0.78 mm, and loss tangent of 0.0009. The termination impedances of the nonreciprocal filtering power divider are chosen as 50 Ω for measurement simplicity using a two-port vector network analyzer. The nonreciprocal filtering power dividers are designed to have equiripple bandwidth of 100 MHz with center frequency tunability between 1.60 and 2 GHz. The RF design of these prototypes starts with the methodology detailed in Section II. Once the required coupling coefficients are obtained using the provided design equations, the resonators are implemented with varactor-loaded quarter wavelength microstrip line time-modulated resonators [24]. The varactor diode used in this work is the SMV-1233 from Skyworks, Irvine, CA, USA, which provides variable capacitance from 1 to 20 pF under reverse dc-bias voltage ranges from 15 to 0 V. The coupling m_{s01} and m_{s02} are implemented with quarter wave TLs. Likewise, coupling m_{01}, m'_{01}, and m_{23} are implemented with coupled lines, whereas m_{12}, m_{3L2}, and m_{3L3} are implemented with short-circuited stub [25]. The modulation signal is directly applied to the varactor diode through TL, which simplifies the modulation circuit by eliminating the need

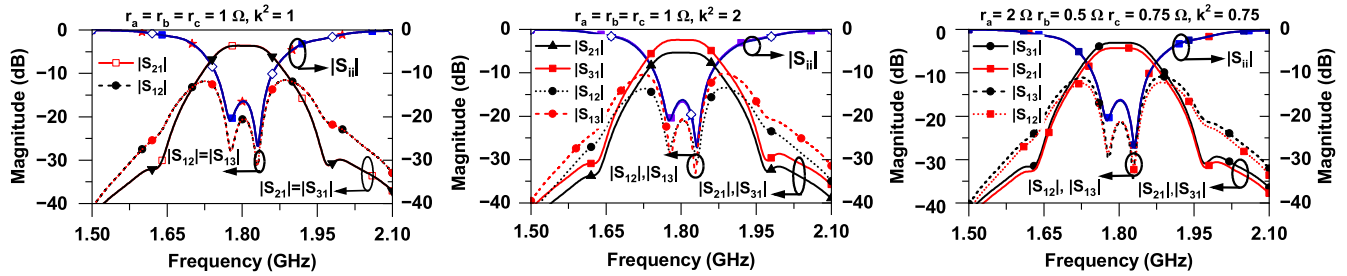

Fig. 6. Numerical simulated frequency response of nonreciprocal filtering power divider with different power division ratio (k^2) and arbitrary termination impedances. Other specifications: $f_0 = 1.8$ GHz, $\Delta = 100$ MHz, and LPF prototype values: $g_0 = g_4 = 0.84985$, $g_1 = g_3 = 0.8635$, and $g_2 = 1.1038$. Modulation parameters: $f_m = 102$ MHz, $\xi = 0.10$, and $\Delta\varphi = 60°$.

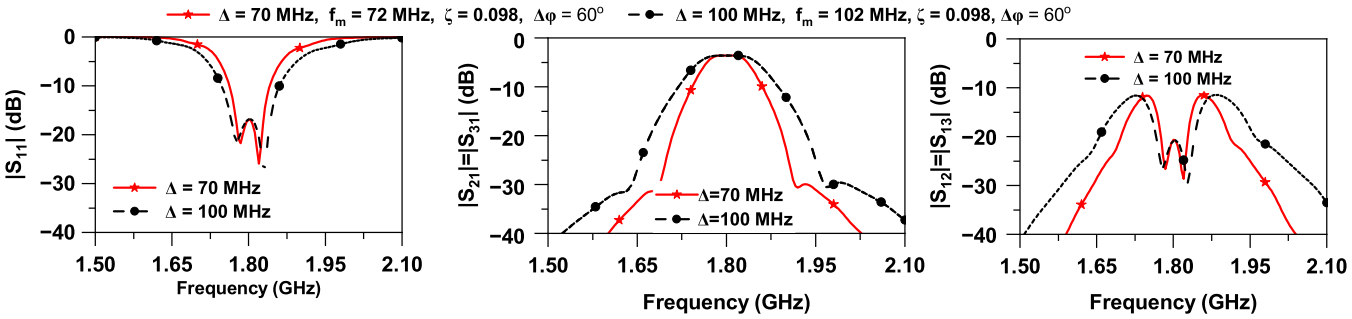

Fig. 7. Numerical simulated frequency response of nonreciprocal filtering power divider with different equiripple bandwidth (Δ). Other specifications: $f_0 = 1.80$ GHz and LPF prototype values: $g_0 = g_4 = 0.84985$, $g_1 = g_3 = 0.8635$, and $g_2 = 1.1038$.

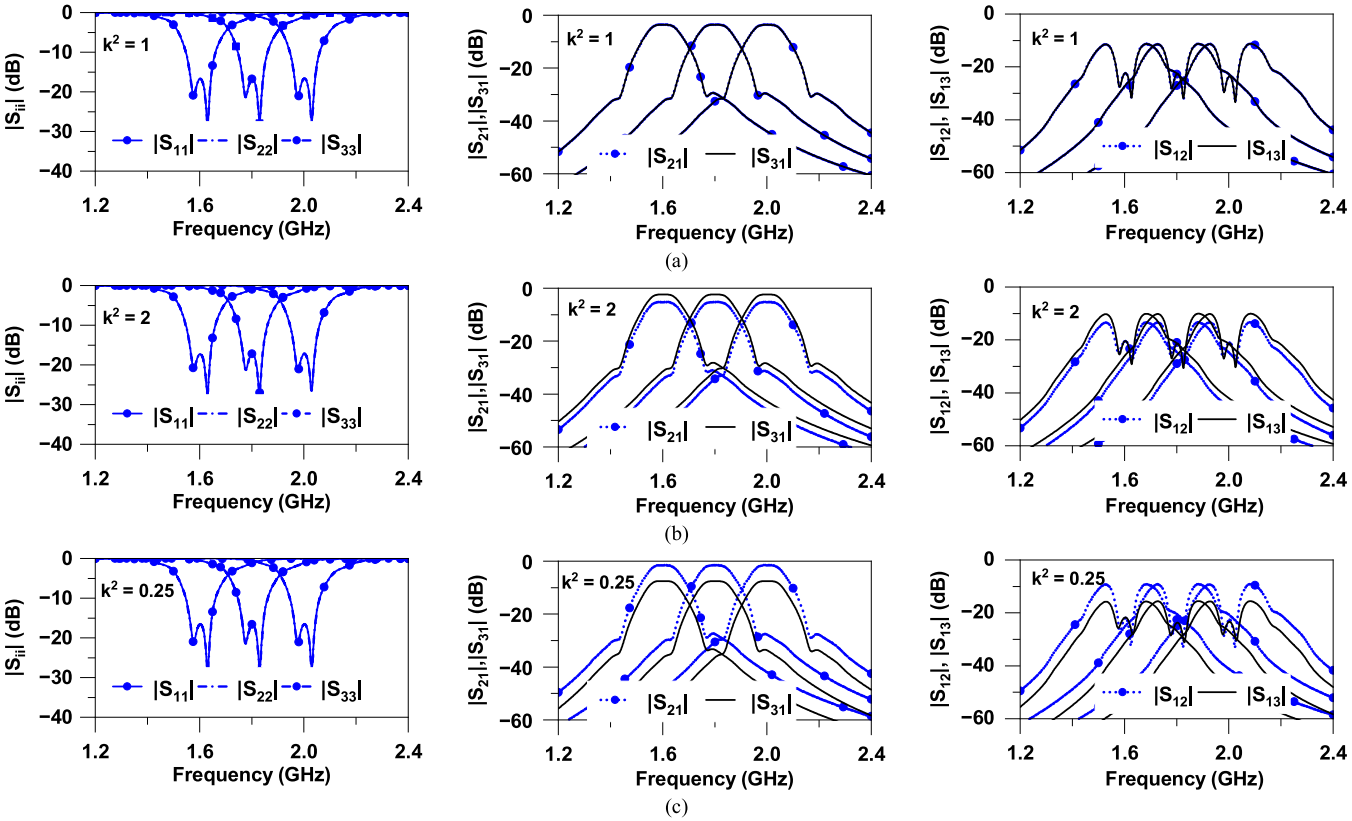

Fig. 8. Numerical simulated frequency response of the proposed nonreciprocal filtering power divider with tunable center frequency: (a) $r_a = r_b = r_c = 1\ \Omega$ and $k^2 = 1$; (b) $r_a = r_b = r_c = 1\ \Omega$ and $k^2 = 2$; and (c) $r_a = 2\ \Omega$, $r_b = 0.5\ \Omega$, $r_c = 0.75\ \Omega$, and $k^2 = 0.25$. Other specifications: $f_0 = 1.6$–2 GHz and $\Delta = 100$ MHz, and LPF prototype values: $g_0 = g_4 = 0.84985$, $g_1 = g_3 = 0.8635$, and $g_2 = 1.1038$. Modulation parameters: $f_m = 102$ MHz, $\zeta = 0.10$, and $\Delta\varphi = 60°$.

separate LPF and other components. High isolation between the RF port and modulation signal source is achieved by controlling the length and width of TL. This approach can reduce the circuit complexity.

The physical dimensions are optimized using co-simulation between Keysight Advanced Design System (ADS) and ANSYS HFSS co-junction with large signal scattering parameters. For simulation, we used the SPICE equivalent circuit

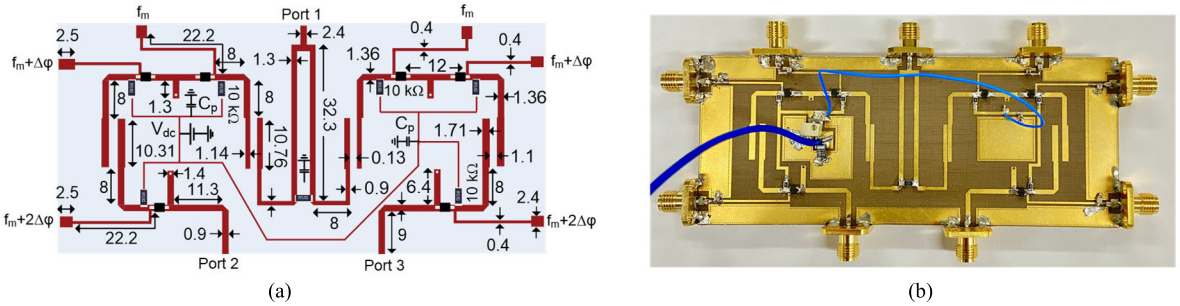

Fig. 9. (a) Physical layout with dimensions and (b) photograph of fabricated filtering nonreciprocal power divider with $r_a = r_b = r_c = 1\ \Omega$ and $k^2 = 1$. Physical dimensions unit: millimeter (mm). Varactor diode: SMV-1233 from Skyworks Inc.

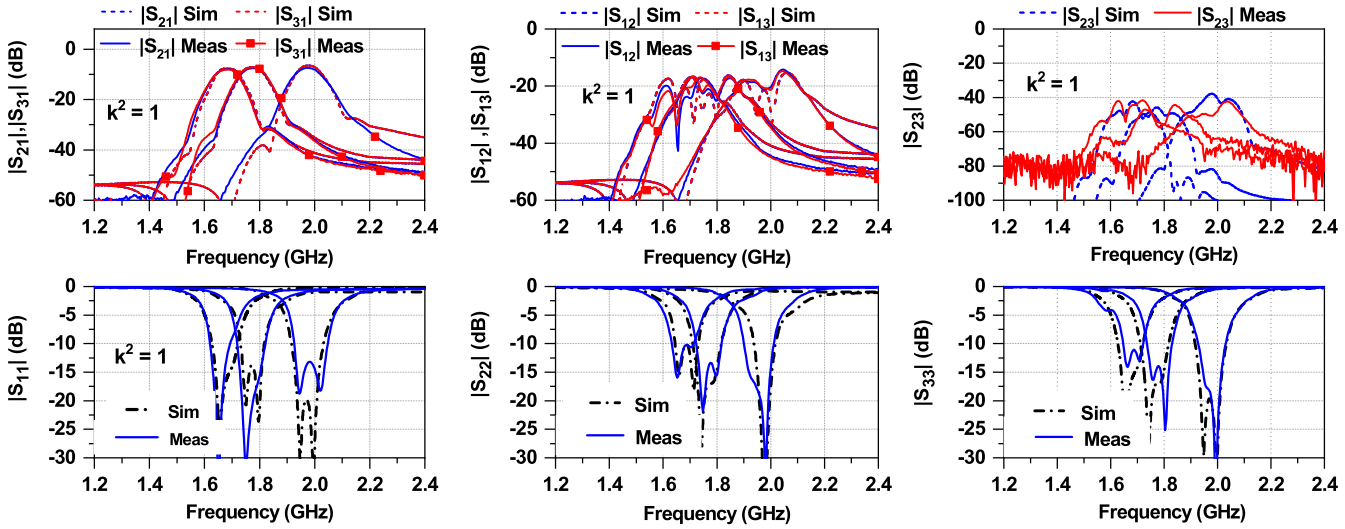

Fig. 10. Simulation and measurement results of filtering nonreciprocal power divider with $k^2 = 1$. Dashed line: simulation and solid lines: measurement.

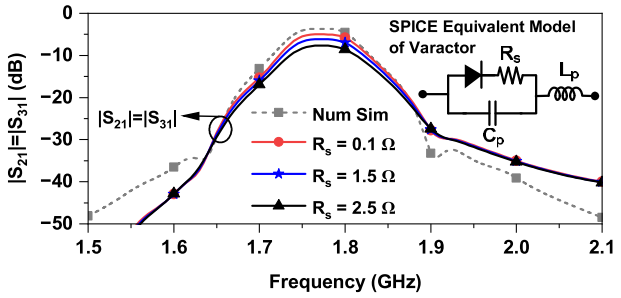

Fig. 11. Simulation results of nonreciprocal power divider with $k^2 = 1$ and different values of parasitic resistance R_s in SPICE model of varactor SMV-1233-079LF. Other parasitic parameters of varactor diode: $C_p = 0.5$ pF and $L_p = 0.7$ nH [29].

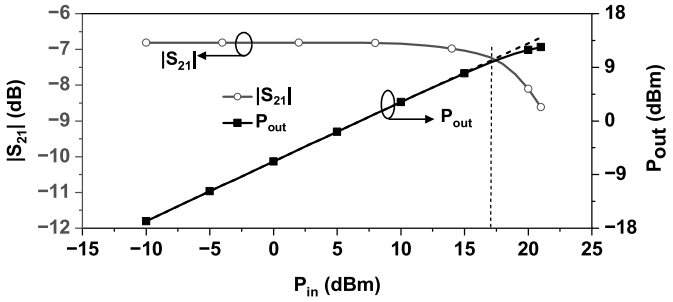

Fig. 12. Measured power handling capability of the proposed nonreciprocal power divider with $k^2 = 1$ and single-tone RF signal at 1.78 GHz.

model of varactor SMV-1233 provided by the manufacturer [29]. The RF characterization was performed through S-parameter measurement using a Keysight N5224A vector network analyzer.

A. Prototype 1: Equal Power Division Ratio $k^2 = 1$

Fig. 9(a) shows the physical layout of the nonreciprocal filtering power divider with $k^2 = 1$. The photograph of the fabricated circuit is shown in Fig. 9(b). Fig. 10 shows the comparison of the simulation and measurement results, which show close agreement between them. The measurement results are summarized in Table I. The nonreciprocal response is achieved by modulating resonators with progressive phase-shifted sinusoidal signal. The isolation between the RF signal port and the modulation signal source is higher than 26 dB.

As seen from these results, the center frequency is tuned from 1.66 to 1.98 GHz with a frequency tunable range (FTR) of 17.58% by changing the bias voltage of varactor. The forward IL degrades when f_0 is tuned toward a lower value. As the dc-bias voltage is changed to a lower value, the parasitic resistance of the varactor diode increases. The degradation in IL is mainly due to the parasitic series

TABLE I
MEASUREMENT RESULTS OF NONRECIPROCAL POWER DIVIDER

Power division ratio		$k^2 = 1$			$k^2 = 0.5$		
Modulation parameters	V_{dc} (V)	1.60	2.70	4.20	1.61	2.72	4.30
	f_m (MHz)	85	85	85	85	85	85
	V_m (V)	1.21	1.10	1.31	1.22	1.12	1.33
	$\Delta\varphi$ (Deg)	60	60	60	60	60	60
	f_0 (GHz)	1.66	1.78	1.98	1.66	1.78	1.98
Measured Results	$\|S_{21}\|$ (dB)	-7.93	-7.10	-6.69	-6.71	-5.96	-5.56
	$\|S_{12}\|$=IX (dB)	-24.03	-21.97	-21.17	-22.55	-20.67	-19.50
	$\|S_{31}\|$ (dB)	-7.98	-7.14	-6.72	-9.82	-9.01	-8.65
	$\|S_{13}\|$=IX (dB)	-21.10	-20.65	-20.68	-24.18	-22.34	-20.68
	$k^2 = \|S_{21}\|/\|S_{31}\|$ (dB)	0.05	0.04	0.03	3.11	3.05	3.09
	$\|S_{23}\|$ (dB)	-44.57	-57.44	-50.63	-44.57	-57.44	-50.63
	$BW_{20dB\text{-}IX}$ (MHz)	96	87	70	92	96	68
	Input/output RL (dB)	> 11.44	> 13.4	> 13.2	> 11.59	> 13.4	> 13.2

IL : Forward transmission insertion loss excluding the intrinsic loss of power divider, IX: reverse isolation = magnitude of $|S_{12}|$ and $|S_{13}|$

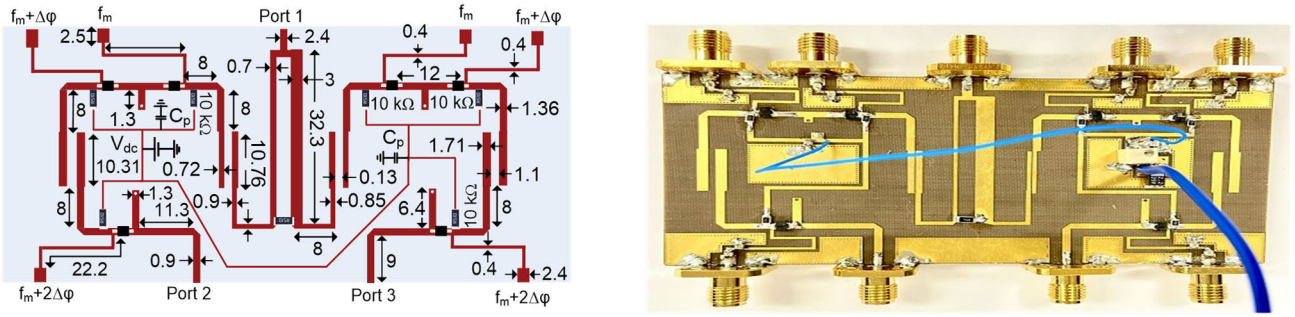

(a) (b)

Fig. 13. (a) Physical layout with dimensions and (b) photograph of fabricated nonreciprocal filtering power divider with $r_a = r_b = r_c = 1\ \Omega$ and $k^2 = 0.5$. Physical dimensions unit: millimeter (mm). Varactor diode: SMV-1233 from Skyworks Inc.

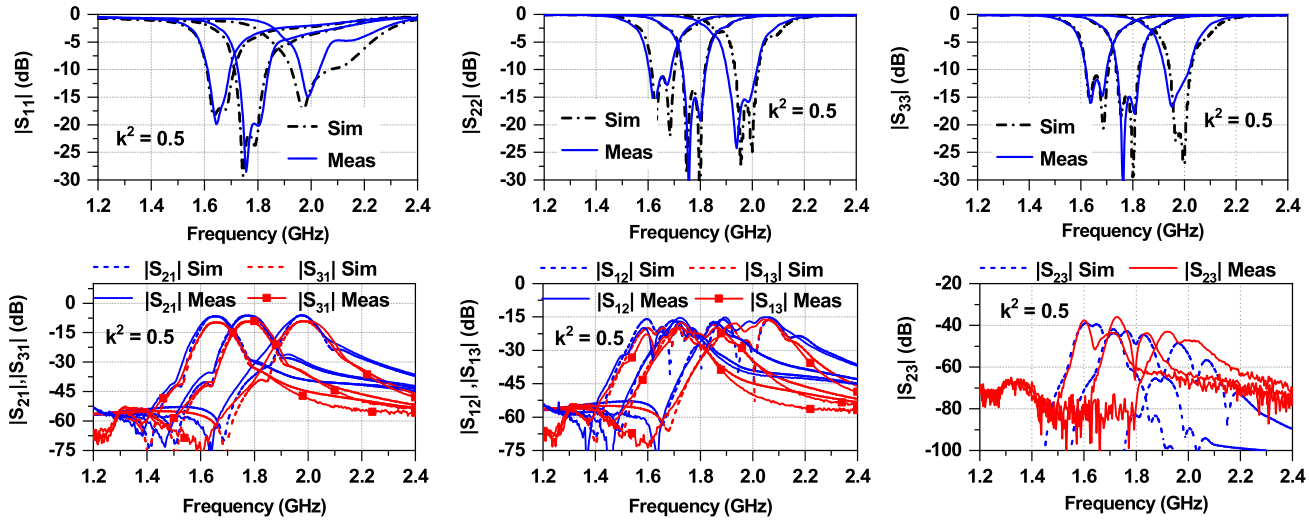

Fig. 14. Simulation and measurement result of nonreciprocal filtering power divider with $k^2 = 0.5$. Dashed line: simulation and solid lines: measurement.

resistance of the varactor diode. The amplitude and phase imbalance are better than 0.27 dB and 0.5° within the passband frequency.

To investigate the cause of the forward transmission IL, we performed a simulation of a nonreciprocal power divider using SPICE model of varactor diode SMV-1233, and the results are shown in Fig. 11. As seen from these results, the forward transmission IL is mainly due to a fraction of interharmonic spectral power conversion to IM products and parasitic resistance (R_s) of varactor diode. A fraction of interharmonic spectral power conversion to IM products generates IL of 0.67 dB, and the rest of IL is due to parasitic resistance R_s of the varactor diode. As the value of R_s increases, the forward transmission IL also increases. The IL can be improved if

TABLE II
PERFORMANCE COMPARISON BETWEEN THE PROPOSED AND PREVIOUSLY REPORTED WORKS

	f_0 (GHz)	k^2	IL (dB)	$BW_{20dB\text{-}IX}$ (MHz)	CF	A
[17]	0.19	NA	1.50	20	No	No
[18]	0.136~0.163	NA	3.7 ~ 4.1	NA	Yes	No
[19]	0.27 ~ 0.31	NA	1.7 ~ 4.3	NA	Yes	No
[20]	0.150	NA	1.5	NA	No	No
[21]	0.96	NA	4.50	N/A	No	No
[22]	1.02	NA	5.50	NA	No	No
[23]	0.88~1.03	NA	4.6 ~ 3.9	42	Yes	No
[24]	1.64 ~1.97	NA	3.94 ~ 4.92	54 ~ 72	No	No
[25]	1.46	NA	3.10	50	Yes	Yes
[27]	2.45	1	8	NA	No	No
This work	**1.66 ~ 1.98**	**1**	**3.72 ~ 4.97**	**70 ~ 96**	**Yes**	**Yes**
	1.66 ~ 1.98	**0.5**	**3.88 ~ 5.04**	**68 ~ 92**	**Yes**	**Yes**

CF: Center frequency tunability
IL: Forward transmission insertion loss excluding intrinsic insertion loss of power divider.
k^2 = Arbitrary power division ratio of power divider
A: Arbitrary termination impedances ($r_a \neq r_b \neq r_c$)
IX= Magnitude of $|S_{12}|$ and $|S_{13}|$ = reverse isolation
$BW_{20dB\text{-}IX}$: 20-dB reverse isolation ($|S_{12}|$, $|S_{13}|$)) bandwidth.

a varactor diode with low parasitic resistance (high Q-factor varactor diode) is used.

The power handling capability of the proposed nonreciprocal filtering power divider is mainly limited by the nonlinearity of varactor diodes. Fig. 12 shows the measured 1-dB compression point ($P_{1\,dB}$) with a single-tone RF signal at 1.78 GHz. As observed from the result, the forward transmission IL ($|S_{21}|$) is degraded when input power (P_{in}) is higher than 16 dBm, providing $P_{1\,dB}$ of the proposed nonreciprocal power divider is approximately equal to 16.1 dBm.

B. Prototype 2: Unequal Power Divider Ratio $k^2 = 0.5$

Fig. 13 shows the physical layout and a photograph of the manufactured nonreciprocal filtering power divider with $k^2 = 0.5$. The simulated and measured S-parameters are shown in Fig. 14, and the measurement results are in good agreement with the simulation. The measurement results are summarized in Table I. The isolation between the RF port and modulation signal source is higher than 26.2 dB. In the experimental results, the center frequency is tuned from 1.66 to 1.97 GHz (FTR = 17.58%) by changing the bias voltage of the varactor diode. The forward IL varies from 3.88 to 5.04 dB (excluding intrinsic IL of the power divider), mainly due to parasitic components of the varactor diode. The reverse IX ($|S_{12}|$ and $|S_{13}|$) is better than 20 dB at each tuning center frequency. The amplitude and phase imbalance are better than 0.5 dB and 1° within the passband frequency.

The performance comparison between the proposed work and previously reported works is shown in Table II. Notably, all previously demonstrated were nonreciprocal BPFs except [27]. Zang et al. [27] demonstrated a microstrip line nonreciprocal filtering power divider with an equal power division ratio. In contrast, the proposed work demonstrates a frequency tunable nonreciprocal filtering power divider with an arbitrary power ratio and arbitrary termination port impedances. The proposed filtering power divider combines multifunctionalities (e.g., frequency tunable filter, arbitrary power division ratio power divider/combiner, and isolator) into a single device.

IV. CONCLUSION

In summary, this article presents the design and practical implementation of a nonreciprocal filtering power divider with an arbitrary power division ratio and tunable center frequency. The analytical spectral S-parameters of the nonreciprocal filtering power divider, which is capable of arbitrary power division ratio and arbitrary termination port impedances, have been derived and validated through numerical simulation and manufactured prototypes. For experimental validation, prototypes of tunable center frequency filtering power divider with equal and unequal power division ratio have been designed, manufactured, and measured. The measured results are in good agreement with the simulated results, and the proposed circuit combines the functionalities of a tunable filter, power divider/combiner, and isolator within a single circuit.

REFERENCES

[1] K. Park, J. Myeong, G. M. Rebeiz, and B. Min, "A 28-GHz full-duplex phased array front-end using two cross-polarized arrays and a canceller," *IEEE Trans. Microw. Theory Techn.*, vol. 69, no. 1, pp. 1127–1135, Jan. 2021.
[2] S. Hong et al., "Applications of self-interference cancellation in 5G and beyond," *IEEE Commun. Mag.*, vol. 52, no. 2, pp. 114–121, Feb. 2014.
[3] J. Zhou et al., "Integrated full duplex radios," *IEEE Commun. Mag.*, vol. 55, no. 4, pp. 142–151, Apr. 2017.
[4] J. W. Zang, A. Alvarez-Melcon, and J. S. Gomez-Diaz, "Nonreciprocal phased-array antennas," *Phys. Rev. Appl.*, vol. 12, no. 5, pp. 054008-1–054008-20, Nov. 2019.
[5] J. T. S. Do, J. Zang, A. Alvarez-Melcon, and J. S. Gomez-Diaz, "Time-modulated patch antennas with tunable and nonreciprocal polarization response," *IEEE Access*, vol. 10, pp. 59057–59067, 2022.
[6] N. Reiskarimian, A. Nagulu, T. Dinc, and H. Krishnaswamy, "Nonreciprocal electronic devices: A hypothesis turned into reality," *IEEE Microw. Mag.*, vol. 20, no. 4, pp. 94–111, Apr. 2019.
[7] C. E. Fay and R. L. Comstock, "Operation of the ferrite junction circulator," *IEEE Trans. Microw. Theory Techn.*, vol. MTT-13, no. 1, pp. 15–27, Jan. 1965.
[8] C. K. Seewald and J. R. Bray, "Ferrite-filled antisymmetrically biased rectangular waveguide isolator using magnetostatic surface wave modes," *IEEE Trans. Microw. Theory Techn.*, vol. 58, no. 6, pp. 1493–1501, Jun. 2010.
[9] S. Tanaka, N. Shimomura, and K. Ohtake, "Active circulators—The realization of circulators using transistors," *Proc. IEEE*, vol. 53, no. 3, pp. 260–267, Mar. 1965.
[10] T. Kodera, D. L. Sounas, and C. Caloz, "Magnetless nonreciprocal metamaterial (MNM) technology: Application to microwave components," *IEEE Trans. Microw. Theory Techn.*, vol. 61, no. 3, pp. 1030–1042, Mar. 2013.
[11] C. Caloz, A. Alù, S. Tretyakov, D. Sounas, K. Achouri, and Z.-L. Deck-Léger, "Electromagnetic nonreciprocity," *Phys. Rev. Appl.*, vol. 10, no. 4, Oct. 2018, Art. no. 047001.
[12] N. A. Estep, D. L. Sounas, and A. Alù, "Magnetless microwave circulators based on spatiotemporally modulated rings of coupled resonators," *IEEE Trans. Microw. Theory Techn.*, vol. 64, no. 2, pp. 502–518, Feb. 2016.
[13] A. Kord, D. L. Sounas, Z. Xiao, and A. Alù, "Broadband cyclic-symmetric magnetless circulators and theoretical bounds on their bandwidth," *IEEE Trans. Microw. Theory Techn.*, vol. 66, no. 12, pp. 5472–5481, Dec. 2018.
[14] Y. Yu et al., "Radio frequency magnet-free circulators based on spatiotemporal modulation of surface acoustic wave filters," *IEEE Trans. Microw. Theory Techn.*, vol. 67, no. 12, pp. 4773–4782, Dec. 2019.
[15] A. Kord, D. L. Sounas, and A. Alù, "Pseudo-linear time-invariant magnetless circulators based on differential spatiotemporal modulation of resonant junctions," *IEEE Trans. Microw. Theory Techn.*, vol. 66, no. 6, pp. 2731–2745, Jun. 2018.

[16] N. Reiskarimian and H. Krishnaswamy, "Magnetic-free non-reciprocity based on staggered commutation," *Nature Commun.*, vol. 7, no. 1, p. 11217, Apr. 2016.
[17] X. Wu, X. Liu, M. D. Hickle, D. Peroulis, J. S. Gómez-Díaz, and A. Á. Melcón, "Isolating bandpass filters using time-modulated resonators," *IEEE Trans. Microw. Theory Techn.*, vol. 67, no. 6, pp. 2331–2345, Jun. 2019.
[18] D. Simpson and D. Psychogiou, "Magnet-less non-reciprocal bandpass filters with tunable center frequency," in *Proc. 49th Eur. Microw. Conf. (EuMC)*, Oct. 2019, pp. 460–463.
[19] D. Simpson and D. Psychogiou, "Fully-reconfigurable non-reciprocal bandpass filters," in *IEEE MTT-S Int. Microw. Symp. Dig.*, Aug. 2020, pp. 807–810.
[20] P. Dutta, G. A. Kumar, and G. Ram, "Numerical design of non-reciprocal bandpass filters with the aid of 3D coupling matrix for 5G bands," *IEEE Trans. Circuits Syst. II, Exp. Briefs*, vol. 69, no. 7, pp. 3334–3338, Jul. 2022.
[21] A. Alvarez-Melcon, X. Wu, J. Zang, X. Liu, and J. S. Gomez-Diaz, "Coupling matrix representation of nonreciprocal filters based on time-modulated resonators," *IEEE Trans. Microw. Theory Techn.*, vol. 67, no. 12, pp. 4751–4763, Dec. 2019.
[22] X. Wu, M. Nafe, A. A. Melcón, J. S. Gómez-Díaz, and X. Liu, "A non-reciprocal microstrip bandpass filter based on spatio-temporal modulation," in *IEEE MTT-S Int. Microw. Symp. Dig.*, Jun. 2019, pp. 9–12.
[23] X. Wu, M. Nafe, A. Á. Melcón, J. S. Gómez-Díaz, and X. Liu, "Frequency tunable non-reciprocal bandpass filter using time-modulated microstrip $\lambda_g/2$ resonators," *IEEE Trans. Circuits Syst. II, Exp. Briefs*, vol. 68, no. 2, pp. 667–671, Feb. 2021.
[24] G. Chaudhary and Y. Jeong, "Frequency tunable impedance matching nonreciprocal bandpass filter using time-modulated quarter-wave resonators," *IEEE Trans. Ind. Electron.*, vol. 69, no. 8, pp. 8356–8365, Aug. 2022.
[25] G. Chaudhary and Y. Jeong, "Nonreciprocal bandpass filter using mixed static and time-modulated resonators," *IEEE Microw. Wireless Compon. Lett.*, vol. 32, no. 4, pp. 297–300, Apr. 2022.
[26] M. Q. Dinh and M. T. Le, "Non-reciprocal diplexer and power combiner/divider from topological cavities with both splitting and combining functions," *AIP Adv.*, vol. 12, no. 4, Apr. 2022, Art. no. 045112, doi: 10.1063/5.0085979.
[27] J. Zang, S. Wang, A. Alvarez-Melcon, and J. S. G. Diaz, "Nonreciprocal filtering power dividers," *AEU, Int. J. Electron. Commun.*, vol. 132, Apr. 2021, Art. no. 153609, doi: 10.1016/j.aeue.2021.153609.
[28] R. J. Cameron, C. M. Kudsia, and R. R. Mansour, *Microwave Filters for Communication Systems: Fundamentals, Design and Applications*. New York, NY, USA: Wiley, 2007.
[29] *SMV123x Series: Hyperabrupt Junction Tuning Varactors*, Skyworks Solutions, Irvine, CA, USA, Nov. 2018.

Girdhari Chaudhary (Member, IEEE) received the B.E. degree in electronics and communication engineering from Nepal Engineering College (NEC), Kathmandu, Nepal, in 2004, the M.Tech. degree in electronics and communication engineering from MNIT, Jaipur, India, in 2007, and the Ph.D. degree in electronics engineering from Jeonbuk National University, Jeonju, Republic of Korea, in 2013.

He worked as a Principal Investigator on an independent project through the Basic Science Research Program administrated by the National Research Foundation (NRF) and funded by the Ministry of Education. He is currently working as a Contract Professor with the JIANT-IT Human Resource Development Center (HRDC), Jeonbuk National University. His research interests include multiband tunable passive circuits, nonreciprocal microwave and millimeter-wave circuits, in-band full-duplex systems, high-efficiency power amplifiers, and applications of negative group delay circuits.

Dr. Chaudhary received the BK21 PLUS Research Excellence Award 2015 by the Korean Ministry of Education and Korean Research Fellowship (KRF) through the NRF funded by the Ministry of Science and ICT.

Yongchae Jeong (Senior Member, IEEE) received the B.S.E.E., M.S.E.E., and Ph.D. degrees in electronics engineering from Sogang University, Seoul, Republic of Korea, in 1989, 1991, and 1996, respectively.

From 1991 to 1998, he worked as a Senior Engineer with Samsung Electronics, Seoul. In 1998, he joined the Division of Electronics Engineering, Jeonbuk National University, Jeonju, Republic of Korea. From July 2006 and December 2007, he worked as a Visiting Professor with the Georgia Institute of Technology, Atlanta, GA, USA. He is currently a Professor with Jeonbuk National University, and had served as the Director of the HOPE-IT Human Resource Development Center of BK21 PLUS and Jeonbuk National University's Vice-President of planning. He has authored or coauthored over 260 articles in international journals and conference proceedings. His research interests include active and passive microwave circuits for mobile and satellite base-station RF system, periodic-defected transmission lines, negative group delay circuits and their applications, in-band full-duplex radio, and RFIC design.

Prof. Jeong is a member of the Korea Institute of Electromagnetic Engineering and Science (KIEES).